

A Genetic Approach to the History of the Magellanic Clouds

Magda Guglielmo*, Geraint F. Lewis, Joss Bland-Hawthorn

Sydney Institute for Astronomy, School of Physics, A28, The University of Sydney, NSW 2006, Australia

Accepted -. Received -; in original form -

ABSTRACT

The history of the Magellanic Clouds is studied by using a genetic algorithm combined with full N-Body simulations. We explore the parameter space of the interaction between the Magellanic Clouds and the Milky Way, considering as free parameters the proper motions of the Magellanic Clouds, as well as the virial mass and the concentration parameter (c) of the Galactic dark matter halo. The use of c as a free parameter is based on recent results which support a low mass halo ($\leq 10^{12} M_{\odot}$) with a higher concentration than assumed in earlier work. We investigate the consequences of such models on the orbital history of the Clouds. The best orbital scenarios presented here are carried out with two different models for the Milky Way disc and bulge components. The total circular velocity at the position of the Sun ($R_{\odot} = 8.5$ kpc) is directly calculated from the rotation curve of the corresponding Galactic mass model. Results of our analysis suggest that the Magellanic Clouds have orbited inside the virial radius of the Milky Way for at least 3 Gyr, even for the low halo mass found in recent work. However this is possible only with high values for the concentration parameter ($c \geq 20$). In both Milky Way models, the Cloud interaction reproduces the observed structures of the Magellanic Stream, with a mean distance of ~ 80 kpc along the South Galactic Pole going to greater distances at larger Magellanic longitudes.

Key words: Magellanic Clouds– Milky Way–N-body Simulation–Genetic Algorithm.

INTRODUCTION

The formation and evolution of galaxies is perhaps the most outstanding problem in astrophysics. According to the Cold Dark Matter paradigm, galaxies form hierarchically, starting from the collapse of the initial Gaussian density fluctuations and then grow by accretion and merging of smaller proto-systems. Imprints of the past merger events are enclosed within the present day galaxies and they can be revealed by studying the baryonic component of their substructures.

For this reason, the study of the Galaxy and its components is crucial for understanding galaxy evolution in the Universe. Studying stellar populations in the halo of the Milky Way, it is possible to unravel some of the formation and evolution history of our Galaxy and to connect its history with the observed high-redshift universe (Freeman & Bland-Hawthorn 2002). Helping us on this archaeological journey, the dwarf galaxies surrounding the Milky Way are plausible ‘building blocks’ that can be used to test the current paradigm of galaxy formation. These satellites are interacting with each other and with the host potential, offering the opportunity to retrace their evolutionary tracks by integrating their respective orbits backwards through time (Murai & Fujimoto 1980).

But there are inconsistencies between the observed properties of galaxies and their satellites that cast doubt on whether dwarfs

are substantial contributors to galaxy formation (Tosi 2003). Several discrepancies between theory and observation seem to support the idea that other mechanisms play important roles in galaxies formation, not fully considered in the hierarchical scenario. For example, Λ CDM simulations overestimate the number of satellites orbiting the Milky Way (*missing satellites problems*) and, at the same time, they underpredict the number of massive satellites, such as the Magellanic Clouds.

Within ~ 100 kpc, these are the most massive satellites in the Local Group and can be seen as a challenge for the current paradigm of galaxy formation. Due to their close distance to the host and their high mass, the Magellanic Clouds represent a peculiarity of the Local Group. In fact, results from both cosmological simulations and observations based on the SDSS show that the presence of two massive star forming galaxies so close to their host is rare (Busha et al. 2011; James & Ivory 2011; Liu et al. 2011; Tollerud et al. 2011; Robotham et al. 2012).

Over the past four decades, many groups have attempted to explain the presence of gas structures which characterise the Magellanic system: the Magellanic Stream and the Leading Arm. This difficult challenge is widely recognized as a benchmark for testing the usefulness of galaxy simulation codes (Bland-Hawthorn et al. 2007). Formerly, the formation of these structures was explained as the result of multiple encounters between these satellites and the Milky Way, after which the gas within the Clouds was stripped by tidal forces (Lin & Lynden-Bell 1977; Gardiner et al. 1994) or ram pressure (Mastropietro et al. 2005; Moore & Davis 1994).

* E-mail: m.guglielmo@physics.usyd.edu.au

However, the new proper motion measurements (Kallivayalil et al. 2006,?) show that the Clouds are on more energetic orbits, making the possibility of multiple encounters with the Galaxy more unlikely. Using the proper motion measurement from the Hubble Space Telescope (Kallivayalil et al. 2006), Besla et al. (2007) show the Large Magellanic Cloud (hereafter LMC) is more likely on its first passage around the Milky Way. Later, they extended this analysis to include the Small Magellanic Cloud (SMC), in order to explain the formation of the Magellanic Stream and the Leading Arm (Besla et al. 2010, 2012). According to the first infall scenario, the Magellanic Stream and the Leading Arm are formed by interactions between the Clouds, while the Milky Way has a secondary role. This model is based on the assumption that the Clouds formed a bound pair before falling into the Milky Way potential (Nichols et al. 2011).

These results, and those regarding the uniqueness of Magellanic Clouds-Milky Way systems, raise the possibility of a different formation history of the Magellanic Clouds, somewhere outside the Local Group. However, due to the observational uncertainties on the Clouds and the unknowns related to the Milky Way potential, it is not possible to exclude a different scenario for the orbit of the Clouds. Several studies have shown that the circular velocity of the Milky Way is able to increase the number of close encounters between LMC and the Galaxy, especially if the rotational velocity is larger than the standard IAU value (220 km s^{-1}) (Shattow & Loeb 2009; Ruzicka et al. 2010; Diaz & Bekki 2012; Zhang et al. 2012).

Thus the main difficulty in modelling the Magellanic Clouds is the large number of parameters that are required to reconstruct their orbit. Not only are uncertain those parameters directly related to the dwarfs, like the proper motion or their mass, but also the mass and circular velocity of the Milky Way, make it hard to trace back the history of these two galaxies. Different approaches have been proposed to study the parameter space of the Magellanic Clouds. Ruzicka et al. (2007) use a genetic algorithm combined with a restricted N-Body integration scheme (Toomre & Toomre 1972; Theis 1999) to address the formation of the stream. A different method is presented in Diaz & Bekki (2012), where the authors explore a wide range of orbital models and use a multi-component N-Body representation for the only SMC, in order to investigate the tidal effects on its disc and the formation of the main structures in the system. Due to the particular integration scheme used, these studies do not fully model the interaction between the Clouds themselves.

In the current paper, we present a genetic algorithm combined with full N-body Gadget2 simulations (Springel 2005), in order to address the formation of the Magellanic System, by exploring different orbits of the Clouds around the Milky Way. The only requirement is that the selected orbits have to reproduce the two encounters between the Clouds in the past 3 Gyr. This is a common feature of all previous models of the Magellanic Clouds orbit, either for the first infall model (Besla et al. 2012) or the more traditional one (Ruzicka et al. 2010; Diaz & Bekki 2012), and traces of these encounters exist in the recent star formation history (SFH) of the Clouds. The presence of two starbursts 2–3 Gyr ago and again $T = 400 \text{ Myr}$, suggest that these two galaxies have interacted in the past (Harris & Zaritsky 2004, 2009). In addition, by using a full N-Body representation for both Clouds, we are able to reproduce the present day distances and velocities of both Clouds, without assuming any *a priori* models of their orbit around each other or around the main host.

This paper is organized as follows: in §1 we present an introduction to the Genetic Algorithm and its application to the Magellanic Clouds problem; in §4 we focus on how the best solution

is selected. In §2 and §3, we describe the numerical model for the Clouds and the Milky Way, as well as the parameters used by the genetic algorithm. In section §5 we provide the orbital models, obtained by using two different sets of parameters for the Milky Way disc and bulge potential. As described in §3, the parameters related to the dark matter halo are instead free to span in the range given by the observational and theoretical constraints. This allows to identify new models for the Milky Way potential in which the Clouds are evolving (§7).

1 WHY DO WE NEED A GENETIC ALGORITHM?

The study of galaxy interactions requires a complete knowledge of the parameters which lead to the observed configuration. The difficulty is that in the case of orbital integration, the parameter space is very large. Just considering the simplest case of two galaxies, it is crucial to know the present day positions and velocities, their total mass and the mass distributions. Adding a third body, such as a central galaxy, increases the number of parameters involved by at least 25 per cent. Therefore, dealing with the problem of multi-body interactions means coping with a higher dimensional space, normally too high for standard approaches, such as Monte Carlo chains.

Emulating the biological concept of evolution, the genetic algorithm (GA) is a powerful tool to explore a complex parameter space. In biology, given a set of possible genetic sequences, which characterises a population of individuals, the fittest organisms are those strong enough to survive and reproduce themselves in their environments: nature selects those creatures having a high probability of survival (“survival of the fittest”). In the optimisation problems, given a set of “possible solutions”, the best is the one which better adapts to the requirements imposed by the model. The genetic algorithm mimics the reproduction, mutation and selection, to arrive at the fittest set of parameters.

Keeping the same terminology from the biological world, a *gene* is the value of a particular parameter and the *phenotype* encodes the collection of all parameters which describe a possible solution. When all the phenotypes are created, they are sorted according to their value of the merit function. A simple genetic algorithm consists of the following steps (Charbonneau 1995):

- (i) Start by randomly generating an initial population of phenotypes, each representing a possible solution.
- (ii) Evaluate the fitness of each member of the current population.
- (iii) Select a pair of genotypes (“parents”) from the current population and breed them, based on their merit. In this way, two new solutions are generated (“offspring”). Repeat this step until the number of offspring produced equals the number of individuals in the current population.
- (iv) Replace the old population with the new one.
- (v) Repeat from step (ii) until the fitness criterion is satisfied.

The evolution process is driven by different types of operators. The first one is the *elitism*: the fittest member of the current population is cloned over the next generation. This guarantees that the maximum values of the fitness function can never fall. The *breeding process* will depend on the selection of the parents: the individuals with highest fitness have higher probability to be selected. When the parents are chosen, a random portion of the genome of one parent is mixed with the corresponding part of the other phenotype; this process is named *crossover*. Whether or not the offspring is

generated will depend on a pre-defined probability (*crossover rate*). The final operation is the *mutation*, which mimics the probability that a particular gene can mutate in the next generation. In the case of a genetic algorithm, the mutation will flip a bit in the phenotype, according to some probabilities determined by the *mutation rate*.

Because of its versatility, the genetic algorithm can be applied to different problems which require exploring a large parameter space. Pioneer work applied this algorithm to different astrophysical problem, such as fitting the light curves and galactic rotation curves (Charbonneau 1995), determination of orbital parameters of interacting galaxies (Wahde 1998), design of filter system (Offer & Bland-Hawthorn 1998) or inversion of gravitational lensed images (Brewer & Lewis 2005).

Using the same recipe described above, we present a genetic algorithm which selects the best individual based on the results of the N-body simulation. The genetic algorithm considers in total six independent parameters: the virial mass and the concentration of the Milky Way halo, the proper motion for LMC and SMC. These parameters will change both the equation of motion and the initial conditions of the Clouds. For each selected value, we used a point mass integration scheme backward in time, so that the correct past position and velocity is assigned to the N-Body representation of both Clouds. Then, the forward integration starts, using Gadget2 simulation code (Springel 2005), which has been modified in order to include a static Milky Way potential. We integrate over a period of 3 Gyr and the last Gadget snapshot (corresponding to the present day configuration) is used to assign the fitness function and so, to select the best individuals.

2 NUMERICAL MODEL

In order to simulate the evolution of the Magellanic Clouds around the Milky Way, we model the latter as a static multicomponent potential, consisting in a disc, a central bulge and a dark matter halo. The disc is assumed to be a Miyamoto-Nagai potential (Miyamoto & Nagai 1975)

$$\Phi_{\text{disc}}(R, z) = -\frac{GM_{\text{disc}}}{\left(R^2 + \left(r_{\text{disc}} + \sqrt{(z^2 + b^2)}\right)^2\right)^{1/2}}, \quad (1)$$

while the bulge component follows a Hernquist profile (Hernquist 1990)

$$\Phi_{\text{bulge}}(r) = -\frac{GM_{\text{bulge}}}{r_{\text{bulge}} + r}. \quad (2)$$

The dark matter halo is given by a Navarro, Frenk and White (Navarro et al. 1997) (hereafter, NFW) potential

$$\Phi_{\text{halo}}(r) = -\frac{GM_{\text{halo}}}{r} \log\left(\frac{r}{r_{\text{halo}}} + 1\right). \quad (3)$$

The halo mass M_{halo} scale is related to the virial mass via

$$M_{\text{halo}} = \frac{M_{\text{vir}}}{\ln(c+1) - c/(c+1)}, \quad (4)$$

and the halo radius r_{halo} is related to the virial radius

$$r_{\text{halo}} = \frac{R_{\text{vir}}}{c}, \quad (5)$$

where c is the concentration parameter.

The initial conditions for the Magellanic Clouds are generated using GalactICS (Kuijken & Dubinski 1995; Widrow & Dubinski 2005; Widrow et al. 2008). Both galaxies are modelled as a

NFW dark matter halo and an exponential disc, using the parameters listed in Table 1. During the initial parameter search, we did not include any gas component for the Clouds. This is because a hydrodynamical simulation will increase the time of a single Gadget run. However, for the best set of parameters found by the GA, a gaseous disc has been added to both the Magellanic Clouds (see section §5.1).

In order to save computational time, the total number of particles used for each run is 10^4 , but for the final results this number increases of a factor of 10. In each galaxy, the number of particles is chosen such that the mass of each particles is roughly the same, respecting the total mass ratio between the Clouds (1:10). Before adding the external potential of the MW, each modelled galaxy has been simulated in isolation in order to test the stability of the system.

3 THE PARAMETER SPACE

Following van der Marel et al. (2002), we adopt a Cartesian coordinate system with the origin at the Galactic centre: the z -axis pointing toward the Galactic north pole, the x -axis pointing from the Sun to the Galactic centre and y -axis aligned in the direction of the Sun's Galactic rotation.

3.1 The Milky Way

The orbital history of the Magellanic Clouds strongly depends on the potential of the Milky Way, in particular on the mass of the dark matter halo. This dependency is not only related to the orbit of the Clouds around their host, but the evolution of the SMC around LMC can change dramatically for a different choice of the Milky Way halo mass.

Due to our position within the Milky Way, it is hard to directly estimate the value for the halo mass. The kinematics of Blue Horizontal Branch in the Galactic halo suggests that the virial mass of the Milky Way is around $10^{12} M_{\odot}$ (Xue et al. 2008; Kafle et al. 2012). Combining the new proper motion measurements of Leo I (Sohn et al. 2013) with numerical simulation of Milky Way-size dark matter halo, Boylan-Kolchin et al. (2013) constrain the mass of the Milky Way's dark matter halo to be $1.6 \times 10^{12} M_{\odot}$ with 90 per cent of confidence in the range $[1.0, 2.4] \times 10^{12} M_{\odot}$. In the following analysis, this parameter is considered as free, assumed to vary between $0.90 \times 10^{12} M_{\odot}$ and $2.0 \times 10^{12} M_{\odot}$.

The dark matter profile in equation 3 depends on the virial radius and concentration parameter, as well as the virial mass. The virial radius, R_{vir} , is calculated for each values of the virial mass, using the equation

$$R_{\text{vir}} = \left(\frac{2M_{\text{vir}}G}{H_0^2\Omega_m\Delta_{th}}\right)^{1/3}, \quad (6)$$

where $H_0 = 70.4 \text{ km s}^{-1} \text{ Mpc}^{-1}$, $\Omega_m = 0.3$ and $\Delta_{th} = 340$. On the contrary, the concentration, c , is considered as free parameter in the range 1 and 30. In previous work the concentration of the halo is considered fixed to be a standard value of 12 (Besla et al. 2012; Diaz & Bekki 2012). By fitting the kinematic of the stellar halo of our Galaxy, recent work by (Kafle et al. 2014, submitted to ApJ) claims that there is the possibility of a more concentrated halo. Therefore, allowing the concentration to vary will allow us to study the consequences of such a model on the orbit of the Clouds.

The circular velocity of the Milky Way at position of the Sun, V_{cir} , influences the orbital history of the Clouds (Shattow & Loeb

2009; Ruzicka et al. 2010). This is because the proper motions are measured relative to the Solar System, so the rotational velocity of the Sun is needed to convert the velocities of the Clouds in a Galactocentric frame (see §3.2). Although the IAU standard value for V_{cir} is 220 km s^{-1} , recent estimations (Reid et al. 2009; McMillan 2011) seem to infer higher values for this parameter. In this work, the circular velocity is directly calculated from the rotation curve of the Milky Way.

Although the disc and the bulge parameters of the Milky Way are not considered here as free parameters, we used two different set of parameters to investigate how the choice of these parameters can influence the orbit of the Clouds. The values for the two different models and their references are listed in table 4.

3.2 Proper Motion

A crucial step for the studying the orbital evolution of galaxies is the choice of their present day velocities. In the last decade, several proper motion catalogues for the Magellanic Clouds have been published (Kallivayalil et al. 2006; Costa et al. 2009; Kallivayalil et al. 2013; Vieira et al. 2010). Even though obtained with different techniques, they are largely consistent with each other. The main problem is that using different values, the orbital history of the Clouds changes completely.

With the aim of selecting the velocity in a more general way, we allow the proper motions to span within the values in Vieira et al. (2010)'s catalogue. This catalogue summarizes the results of CCD and photographic observation of ground based telescope for a baseline of 40 years. The advantage of using this catalogue is to include, within the error, the other proper motion measurements.

Once the proper motions in both directions are selected, the velocities of the Clouds need to be corrected with respect to the position and velocity of the Sun

$$\mathbf{r}_{\odot} = (-R_0, 0, 0), \quad \mathbf{v}_{\odot} = (U_{\odot}, V_{\odot} + V_{\text{cir}}, W_{\odot}), \quad (7)$$

where $(U_{\odot}, V_{\odot}, W_{\odot}) = (11.1, 12.24, 7.25) \text{ kms}^{-1}$ (Schönrich et al. 2010) and the distance of the Sun from the Galactic centre is fixed to be $R_0 = 8.5 \text{ kpc}$.

The proper motion in the direction of west and north are defined as

$$\mu_W = -\cos \delta \frac{d\alpha}{dt}, \quad \mu_N = \frac{d\delta}{dt}, \quad (8)$$

For each values of the proper motions pair selected by the GA, and the total circular velocity at the position of the Sun corresponding to the particular mass model of the Milky Way, the present day velocities are transformed in the Galactocentre frame using

$$v^i = v_{\odot}^i + V_{\text{sys}} u_0^i + D \mu_W u_1^i + D \mu_N u_2^i, \quad (9)$$

where V_{sys} is the line-of-sight systemic velocity and D is the distance of the galaxy, given in Table 2.

The vectors \mathbf{u}_0 , \mathbf{u}_1 and \mathbf{u}_2 are the unit vector from the Sun in the direction of the Clouds and they are given by

$$\begin{aligned} \mathbf{u}_0 &= (\cos l \cos b, \sin l \cos b, \sin b) \\ \mathbf{u}_1 &= -\frac{1}{\cos \delta} \frac{\partial \mathbf{u}_0}{\partial \alpha} \\ \mathbf{u}_2 &= \frac{\partial \mathbf{u}_0}{\partial \delta} \end{aligned}$$

where the Galactic Coordinate (ℓ, b) are those listed in Table 2.

4 THE MERIT FUNCTION

The use of the genetic algorithm, together with the N-Body integration, allows an automatic search in the parameter space, with a simultaneous comparison between model and observations. The choice of the merit function is the most critical step of the algorithm: the wrong function can lead to algorithm to converge to the wrong solution. Following Ruzicka et al. (2010), the total function, F , is defined in such a way that it will return a number in the range 0 and 1, according to the ability of the single individual to satisfy the imposed requirements. Here, F is chosen to be the product of three different functions

$$F = f_1 * f_2 * f_3, \quad (10)$$

each representing a particular requirements.

The first condition is that the final position and velocity of the main body are consistent with the observed values for the Magellanic Clouds. During the N-Body simulation, the formation of particle structures could cause a deviation of the centre of mass orbit from the one calculated with the point mass approximation. This deviation can lead the Clouds to be in the wrong position in the sky. In order to reproduce their present day positions and velocities, a comparison between the simulation results and the observed values is made through the equation

$$f_1 = \prod_{i=1}^{12} \frac{1}{1 + \left(\frac{x_i - x_{i\text{exp}}}{x_{i\text{exp}}} \right)^2} \quad (11)$$

where x_i indicate the (x, y, z) positions and the corresponding velocity components of the centre of mass of each Cloud, as resulting from the N-body integration and $x_{i\text{exp}}$ is the corresponding observed values. To better compare these quantities, the centre of mass is calculated using the only particles bound to the main bodies.

The second condition f_2 is on the orbit of SMC around LMC. As shown by Harris & Zaritsky (2004, 2009), the star formation history of both Magellanic Clouds presents two common peaks at $T \sim 2.5 \text{ Gyr}$ and $T \sim 0.4 \text{ Gyr}$. These can be interpreted as two close encounters between the Clouds. With the aim of reproducing these features, the best parameters are defined in such a way that there have been at least two encounters between SMC and LMC

$$f_2 = \prod_{i=1}^2 \frac{1}{1 + \left(\frac{t_j - T_j}{\sigma} \right)^2} \quad \text{where } j = 1, 2 \quad (12)$$

where t_1 (t_2) is the time of the first (second) encounter and $T_1 = 2.5 \text{ Gyr}$ ($T_2 = 0.4 \text{ Gyr}$) corresponds to the time of the peaks in the star formation of both Clouds (Harris & Zaritsky 2009). Although the values of T_1 and T_2 are well constrained, we noticed that demanding two encounters at fixed time is a very strong condition and the algorithm might require a large number of generations to reach the convergence. In order to release this requirement, we set σ to be 0.5 Gyr .

The last condition is related to the angular velocity at the position of the Sun ($R_{\odot} = 8.5 \text{ kpc}$). The circular velocity is calculated directly from the rotation curve of the Galaxy at R_{\odot} and the peculiar motion of the Sun with the respect to the local standard of rest is $V_{\odot} = 12.24 \text{ km s}^{-1}$ (see §3.2), the f_3 condition in equation 10 is given by

$$f_3 = \frac{1}{1 + \left(\frac{\omega - \Omega_{\text{exp}}}{\sigma} \right)^2}, \quad (13)$$

where $\omega = \frac{(V_{\odot} + V_{\text{cir}})}{R_{\odot}}$ is the angular velocity. The values of Ω_{exp} and σ are such that the angular velocity of each individual belongs to the range $[28.0, 32.0] \text{ km s}^{-1} \text{ kpc}^{-1}$, consistent with the range found by McMillan & Binney (2010).

5 THE BEST ORBITAL MODEL

The genetic algorithm studies the evolution of a first generation, consisting of 50 individuals randomly selected on a sample of possible solutions. The evolution ends when the maximum number of generation reaches 50. The results presented here refer to the best individual (*high fitness value*) in the last generation.

The genetic algorithm does not constraint the Clouds to be bound to each other or to the Milky Way, in order to not impose any strong assumption on the history of these galaxies. Table 3 lists the parameters and the intervals where they are assumed to vary and the best values found by the algorithm for the two different mass model of the Milky Way. The best individuals are described in columns 3 and 4.

As mentioned in section §2, for each run of the genetic algorithm, the Clouds are modelled with a small number of particles and no gas particle are included. However, for the two best solution presented here, a new simulation with Gadget2 is carried out, using the same mass model for the Clouds described in 1, but with a total particle number of 3×10^5 . In this final simulation, a gas component is added to each of the Clouds. It is important to note that the best solution found by the genetic algorithm strongly depends on the particular choice of the Clouds' mass distribution. Therefore, it is important that the total mass of the each Cloud remains the same to the one used in the parameter search. We add a disc of gas, with the mass defined in such a way that the gas fraction (ratio between the mass of the gas and the total baryonic mass) are $f_{\text{gas}} = 0.3$ and $f_{\text{gas}} = 0.7$ for LMC and SMC respectively (Besla et al. 2012). The results presented in the following section referred to those obtained by adding the gas components and a number of particles greater than the one used in the genetic algorithm run.

5.1 Model 1: an initial orbit scenario

For the Milky Way disc and bulge models, we follow the fiducial model used in Besla et al. (2007). The parameters for the Miyamoto-Nagai disc are $M_{\text{disc}} = 5.5 \times 10^{10} M_{\odot}$, $r_{\text{disc}} = 3.5 \text{ kpc}$ and disc scale height given by $r_{\text{disc}}/5.0 \text{ kpc}$. The bulge has a mass of $M_{\text{bulge}} = 1.0 \times 10^{10} M_{\odot}$ and radius of 0.7 kpc . As mentioned in §3.1, the virial radius and the concentration parameters vary in the range defined in Table 3. For the best solution, the virial mass is $0.99 \times 10^{12} M_{\odot}$, virial radius of 256.4 kpc and concentration equals to 27.3 . The final rotation curves for the Milky Way corresponding to this model are shown in the left panel of figure 1. The proper motions for the best individual are

$$(\mu_{\text{W}}, \mu_{\text{N}})_{\text{LMC}} = (-1.87, 0.38) \text{ mas/yr} \quad (14a)$$

$$(\mu_{\text{W}}, \mu_{\text{N}})_{\text{SMC}} = (-1.08, -1.04) \text{ mas/yr} \quad (14b)$$

The orbit around the Milky Way for the above set of parameters is showed in the left column of Figure 2. The first panel described the orbit of the Clouds around the Milky Way, showing that the Clouds are already within the virial radius of the Milky Way 3.0 Gyr ago. At this time, both galaxies are at a distance of 200 kpc from the galactic centre and with a mutual separation of 30 kpc .

The first panel on the second row in Figure 2 provides the orbit of SMC around LMC. The first encounters between the Clouds occurs at $T \approx -2.5 \text{ Gyr}$, when SMC is at 25 kpc away from the centre of LMC. This encounter is strong enough to change the morphology of the gas disc of SMC and a temporary bridge of gas connects the two Clouds. This structure lasts until the SMC starts to moving away from LMC. Before the second encounter, SMC gas particles form arm-like structures. These lead to the formation of the Stream. The second encounter, $T = -0.38 \text{ Gyr}$, is the strongest one, with the Clouds having a distance of 5 kpc to each other. At this time also particles from the SMC disc start to be stripped away from the SMC disk, in the direction of the Leading Arm.

The final configuration of the gas particles is shown in figure 3. As a result of the interaction between the Clouds, the final distribution of particles is such that the main components of the Magellanic Stream are reproduced. Figure 4 shows the line-of-sight distance (*top panel*) and velocity (*bottom panel*) along the simulated Stream as function of the Magellanic Longitude, ℓ_{MS} (Nidever et al. 2008). In both panels, the white star indicates the position of the South Galactic Pole (SGP). The line-of-sight distance increases along the Stream, having a minimum ($d = 62 \text{ kpc}$) at $\ell_{\text{MS}} = -30^{\circ}$. The distance of the Stream at the position of the SGP is 78 kpc .

The analysis of the observed line-of-sight velocity of the Stream as function of the Magellanic Longitude shows the presence of a velocity gradient between $-150^{\circ} \leq \ell_{\text{MS}} \leq -30^{\circ}$, (Putman et al. 2003; Nidever et al. 2010). A clear gradient of the line-of-sight velocity is shown in the bottom panel of Figure 4. The white line shows the fit on the data from Nidever et al. (2010), while the fit on the simulated data is plotted in yellow. The model reproduces the observed velocities range of the full system, with significant agreement with the observed fit.

5.2 Model 2: a better orbit model

In a recent paper, (Kafle et al. 2014, submitted to ApJ) model the kinematic data of the Blue Horizontal Branch and K-giant stars, offering the most recent estimation of the parameters for the components of our Galaxy. Here, we use their estimation of the disk and bulge parameters to construct the model of the Milky Way. According to Kafle (2014), the mass disc is $M_{\text{disc}} = 7.6 \times 10^{10} M_{\odot}$ with scale length of $r_{\text{disc}} = 6.5 \text{ kpc}$ and height equal to 0.26 kpc . The main difference with the previous model is in the bulge, with mass $M_{\text{bulge}} = 2.4 \times 10^{10} M_{\odot}$ and radius 0.31 kpc .

As for the previous model, the mass and the concentration parameter for the dark matter halo are free parameters. For the best solution, these two parameters are $M_{\text{vir}} = 1.27 \times 10^{12} M_{\odot}$ and $c = 20.5$, with a corresponding virial radius of $R_{\text{vir}} = 279 \text{ kpc}$. The rotation curve are plotted in the left panel of figure 1. The chosen proper motion are

$$(\mu_{\text{W}}, \mu_{\text{N}})_{\text{LMC}} = (-2.03, 0.19) \text{ mas/yr} \quad (15a)$$

$$(\mu_{\text{W}}, \mu_{\text{N}})_{\text{SMC}} = (-0.98, -1.20) \text{ mas/yr} \quad (15b)$$

The plots in the second column of figure 2 show the orbit of the Clouds in the last 3 Gyr . This model present several similarity with Model 1, although the mass model of the Galaxy is different. The Clouds are within the virial radius back to 3 Gyr . No close encounters with the Milky Way occur in this time interval, except for the present day distance ($r_{\text{LMC}} = 49.1 \text{ kpc}$ and $r_{\text{SMC}} = 59.1 \text{ kpc}$). The SMC lies on an orbit of 0.62 eccentricity around the Milky Way, while the LMC orbit has eccentricity of 0.64 .

The first encounter between LMC and SMC occurs at $T = -2.6$ Gyr with a distance between them of 36 kpc. Even with a greater separation than the previous model, this encounter is still strong enough to strip away gas from SMC, leading to the formation of a gas tail in the following 2 Gyr. The last encounter at $T = -0.3$ Gyr is more recent than the previous model, but still consistent with the reference values used in equation 13, with a mutual distance between the Clouds of 6 kpc.

The final configuration of the gas particles in Hammer-Aitoff projection is provided in Figure 5. Although there is a clear evidence of the extended tail in the position of the Magellanic Stream, for this model there is not well formed Leading Arm. Figure 6 shows the line-of-sight distance along the stream (*top panel*) and the gradient of the line-of-sight can be seen in the the bottom panel of the same figure. As for Model 1, the distance along the Stream increase as ℓ_{MS} , having a minimum values of 63 kpc at $\ell_{\text{MS}} = -30^\circ$ and a distance of 76 kpc at the SGP.

6 THE ORBIT OF SMC AROUND LMC

As mentioned before, no constrains are imposed on the orbit of the Clouds around the Milky Way or around each other. Using a full N-Body simulation in the analysis of the genetic algorithm helps to discern realistic orbits for the Clouds.

As discussed in Besla et al. (2012), the SMC needs to orbit around the LMC with eccentricity around 0.7 to avoid extreme cases of fly-by or quick orbital decay with subsequent merger. In our analysis, these extreme cases are naturally avoided, since one of the requirements is that the present-day position has to be reproduced for both Clouds (see equation 16). Even if there is not a direct dependency on the eccentricity in the fitness function, the term f_1 indirectly depends on the particular orbit of SMC around LMC, because in both extreme cases the position of the smaller galaxy will be not reproduced, causing low values of the f_1 term. Figure 7 shows an example of the dependency on the eccentricity, as found in the results for Model 1. In this figure, the values of the f_1 terms for all the individuals in each generation are plotted against the eccentricity of the corresponding orbit. The size of the points is scaled according to the value of the total fitness, F , while the color scale indicates the values of the term f_2 , which contains information on the number of encounters between the Clouds and the time when they occurred. Since the f_3 term is related only to the angular velocity, no dependency on the eccentricity has been noticed, therefore the evolution of this term is not included in this analysis.

During the GA generations, orbits with different eccentricity are explored. From the distribution of points shown in figure 7, there is a clear peak around eccentricity between 0.60 – 0.70, corresponding to solutions able to satisfy simultaneously the condition on the encounters between the Clouds and the present day position and velocity. In the very first generations, high eccentricity orbit ($e \sim 0.9$) are analysed, but the low values of the $F = f_1 * f_2$ ensure that these phenotypes do not survive. Orbits with high eccentricity are able to reproduce the present day position and velocity (high values of f_1), but there are no encounters between the Clouds in the first 2 Gyr (low values of f_2), although in all these orbits there is a closer encounter in the last 0.5 Gyr (Kallivayalil et al. 2013). Since the Clouds are not interacting during the integration time, there is not mutual effect on their orbit, due to the dynamical friction between the two haloes. Therefore, there is not deviation on

their orbit, resulting in an almost perfect match with the observed position on the sky.

However, there are solutions where SMC has multiple encounters with LMC and lies on high eccentric orbit. For these particular solutions, the orbit of SMC decays too fast, leading a full merge between the Clouds. The same fate is intended for systems with eccentricities lower than 0.5. The pronounced peak around 0.6-0.7 eccentricity suggests that such SMC orbits necessary to ensure the survival of this Cloud (Besla et al. 2012) and to have two encounters between the Clouds at $T \sim -2.5$ Gyr and $T \sim -0.4$ Gyr (Harris & Zaritsky 2009).

7 FUNDAMENTAL PARAMETERS

7.1 The virial mass of the halo

The debate over the value of the Milky Way virial mass is far from over. Analysis on the kinematics of the stellar halo of our Galaxy lead to constraints on the dark matter in the range $0.91 - 1.5 \times 10^{12} M_\odot$ (Xue et al. 2008; Kafle et al. 2012). On the other hand, dynamical models for the Magellanic Clouds require a more massive halo in order to justify the formation of the Magellanic System. In their study of the parameter space of the Magellanic Clouds, Diaz & Bekki (2012) show that the formation of the Magellanic Stream favours models with virial mass of $\geq 1.3 \times 10^{12} M_\odot$. The results of the orbital implication of the new proper motion catalogue presented in Kallivayalil et al. (2013), support high mass model of the Milky Way for low mass of LMC and SMC ($10^{10} - 10^9 M_\odot$), in order to keep the Clouds bound to each other. In particular they found that in order to keep the Clouds in a binary state the mass of the LMC needs to be as high as $10^{11} M_\odot$, while the Milky Way mass needs to be relative low. The results of this work seem to contradict these constraints on the Milky Way virial mass.

In both models presented, the Clouds formed a binary state at least for a time interval of 3 Gyr. This is crucial for the formation of the Stream. Since both models have no encounters with the Milky Way, the only encounters between the SMC and LMC are strong enough to strip material from SMC, leading the formation of the Stream (Besla et al. 2012). However, while for Model 2 the virial mass corresponding to the best individual is $1.27 \times 10^{12} M_\odot$, the results for Model 1 seem to support model with a lower mass of the main galaxy.

In order to characterise this finding, a set of 50 proper motions has been drawn from the error distribution of the Vieira et al. (2010)'s catalogue. For each of these values, a genetic algorithm ran with a point mass integration scheme. Since all the good orbits found using the N-Body simulation concentrate around an eccentricity of the SMC orbit around LMC between 0.6 – 0.7, the f_1 term in equation 10, has been modified with

$$f_1 = \frac{1}{1 + \left(\frac{e_i - 0.65}{0.05}\right)^2} \quad (16)$$

while the condition on the encounters (f_2) and (f_3) are kept as described in section §4. In each genetic algorithm run, 150 phenotypes evolve for 150 generations. The same analysis has been repeated using the disc and bulge parameters for Model 1 and Model 2.

Once a distribution of the best individuals is established, we use an MCMC estimator to find the most likely values for the virial mass and the concentration and the respective standard deviation. The prior for these two parameters is given by the parameter range described in table 3. The final distribution for Model 1 (virial mass

and concentration) are shown in figure 8. The most likely value for the virial mass for Model 1 (Model 2) is $M_{\text{vir}} = 1.05^{+0.06}_{-0.04} \pm 0.12^{+0.06}_{-0.02} \times 10^{12} M_{\odot}$ ($M_{\text{vir}} = 1.03^{+0.02}_{-0.02} \pm 0.19^{+0.08}_{-0.03} \times 10^{12} M_{\odot}$), showing that solution with a lighter Milky Way halo are preferred. However, this is possible only with higher concentration values. Indeed, the most likely value is $c = 26.2^{+0.8}_{-0.5} \pm 1.5^{+0.2}_{-0.1}$ ($c = 21.7^{+1.4}_{-1.2} \pm 3.3^{+0.6}_{-1.4}$).

Results from numerical simulations show that the mass-concentration relation predicts a mean values for the concentration parameter of 10, when the virial mass is around $10^{12} M_{\odot}$ (Macciò et al. 2008). Both results found by the genetic algorithm appear to overestimate this parameter. However, the relation between virial mass and concentration is based on dark matter simulations, while the presence of baryons can adiabatically contract the dark matter halo, leading for instance to more concentrated haloes (Mo et al. 1998; Gnedin et al. 2004; Rashkov et al. 2013). In addition, the studies of the potential of the Milky Way by its stellar halo, all converge to the conclusion that a virial mass of the dark matter halo ($\leq 10^{12} M_{\odot}$) and high concentration parameter are favoured over the less concentrated-more massive halo model (Battaglia et al. 2005; Deason et al. 2012; Kafle et al. 2014).

7.2 The distance to the Magellanic Stream

The precise distance of the Magellanic Stream has important implications for fundamental parameters of the Stream. For example, the Stream’s total gas mass is critically dependent on its distance (Putman et al. 2003). The detectability of certain stellar populations also depends on the Stream’s distance. No stars have been detected which has hampered distance estimates to date.

One constraint on distance is provided by the geometrical method presented in Jin & Lynden-Bell (2008). Using the data from Putman et al. (2003), they found that the tip of the stream is at a distance of 75 kpc. The top panels in figures 4 and 6 show that in both models the simulated Stream is at a distance greater than the expected one. The discrepancies between the models and the observation are due to the absence of the ram pressure term in modelling the interaction between the gas within the Clouds and the hot halo gas of our Galaxy. The dense Galactic environments will have a strong influence on the inclination and the distance of the Stream. Introducing this interaction, by modelling the Milky Way as a dynamically live galaxy or in the form of a drag force component in the equation of motion, will improve the final shape, inclination of the simulated Stream and the Leading Arm.

The similar trend of the distance as function of ℓ_{MS} , shared by the two models as shown in Figure 9, is particularly interesting. In this figure, the solid lines describe the fit to the simulated Stream for Model 1 (red) and Model 2 (blue), in order to show the trend while the shaded region provide the error on the fit, obtained from the bootstrap distribution. Both models have the similar distance between $-80^{\circ} \leq \ell_{MS} \leq -30^{\circ}$, with equal distance at the position of the South Galactic Pole (black star) of 80 kpc. For $\ell_{MS} < -80^{\circ}$, the increase of the distance is steeper for Model 2 than for Model 1.

An accurate distance for the Stream also bears on resolving a longstanding mystery of the Stream’s high levels of ionisation over the SGP. The presence of bright H α emission around the South Galactic Pole ($\ell_{MS} = -57^{\circ}$) cannot be explained by a Galactic UV radiation field (stars, gas, etc.). In a recent paper, Bland-Hawthorn et al. (2013) argue that the photoionization levels along the Stream are best explained by a Seyfert flare model, consistent with the most viable explanation for the *Fermi* bubbles Guo & Mathews (2012).

Bland-Hawthorn et al. (2013) define an ionization cone emanating from Sgr A* aligned roughly with the South Galactic Pole (SGP) and gas clouds within the cone are lit up by a Seyfert flare approximately 2 Myr ago.

The energetic details of the past explosion depend critically on the distance to the Stream. A near-distance of about 50 kpc lowers the required energetics to about 10 per cent of the maximum Eddington luminosity required by Sgr A*. A greater distance of 100 kpc pushes up the required luminosity close to its maximum value (Bland-Hawthorn et al. 2013, see their Appendix A). For the smaller distance, a shock cascade acting along the Stream could conceivably account for the observed H α emission. But this model breaks down for the larger distance due to the lower halo coronal density (Bland-Hawthorn et al. 2007).

8 CONCLUSION

We present a new and novel technique for the study of the interaction between the Magellanic Clouds and Milky Way. By combining the genetic algorithm with a full N-body simulations, we are able to identify the orbit of the Magellanic Clouds, based on a direct comparison between simulations and observations. Previous studies have constrained the orbital parameters of the MC-MW system (Ruzicka et al. 2009; Diaz & Bekki 2012), but this is the first time that both Clouds have been modelled as a full N-Body system. During the parameter search, the Magellanic Clouds are represented by dark matter halo and a disc components with total mass equal to $2.43 \times 10^{10} M_{\odot}$ for LMC and $0.63 \times 10^{10} M_{\odot}$ for SMC.

The Milky Way is modelled as a 3D component potential, having a Herquist bulge, Miyamoto-Nagai disc and a Navarro, Frenk and White dark matter halo. The latter depends on three parameters: the virial mass, the virial radius and the concentration parameters. In this analysis, the virial mass and concentration are independent parameters, free to span in the range given in table 3, while the virial radius of the dark matter halo is instead directly calculated from the values of its virial mass. Although the dark matter halo has the strongest influence on the motion of the Clouds, the particular choice of disc and bulge parameters influences the value of the Milky Way circular velocity, crucial parameter for the orbit of the Clouds (see equation 9). Therefore, for each selected virial mass and concentration, the circular velocity at the position of the Sun is directly calculated by the rotation curve of the Milky Way.

By using two different models for the disc and bulge of the Milky Way, we provided two orbital scenario for the Clouds. As seen in figure 2, both models support more traditional orbits around the main Galaxy. This is not surprising, since traditional orbits are expected for a $10^{10} M_{\odot}$ mass LMC, in particular with a high ($\sim 245 \text{ kms}^{-1}$, in both models) circular velocity (Zhang et al. 2012; Kallivayalil et al. 2013). Interestingly, the values of the Milky Way parameters describe a less massive ($\leq 1.5 \times 10^{12} M_{\odot}$) but more concentrated dark matter halo ($c > 20$). We show that this is not odd, since studies of the kinematic of the Milky Way stellar halo also prefer such models, with higher concentration parameter than the one obtained by cosmological simulation (Battaglia et al. 2005; Deason et al. 2012).

The orbits described in figure 2 are selected by using the star formation history as the only condition on the LMC-SMC interaction. The two common starbursts, one 2-3 Gyr ago and the other 400 Myr ago, can be interpreted as evidences for two possible encounters between the Clouds (Harris & Zaritsky 2009, 2004). No other orbital criteria are applied, especially on the evolution around

	LMC	SMC
$M_{\text{halo}} (M_{\odot})$	2.13×10^{10}	0.50×10^{10}
$M^* (M_{\odot})$	0.31×10^{10}	0.12×10^{10}
$r_{\text{disc}} (\text{kpc})$	1.4	1.25
$h_{\text{disc}} (\text{kpc})$	4.0	2.0
$r_{\text{halo}} (\text{kpc})$	10	5.0

Table 1. Initial Conditions for LMC and SMC.

Parameter	Value
Model 1 (Besla et al. 2007)	
$M_{\text{disc}} (10^{10} M_{\odot})$	5.5
$r_{\text{disc}} (\text{kpc})$	6.65
$b_{\text{disc}} (\text{kpc})$	$r_{\text{disc}}/5$
$M_{\text{bulge}} (10^{10} M_{\odot})$	1.0
$r_{\text{bulge}} (\text{kpc})$	0.7
Model 2 (Kafle et al. 2014)	
$M_{\text{disc}} (10^{10} M_{\odot})$	7.6
$r_{\text{disc}} (\text{kpc})$	6.5
$b_{\text{disc}} (\text{kpc})$	0.3
$M_{\text{bulge}} (10^{10} M_{\odot})$	
$r_{\text{bulge}} (\text{kpc})$	0.31

Table 4. Disc and Bulge parameters used for the two models for the Milky Way

the Milky Way. As discussed in Besla et al. (2012), not all the LMC-SMC orbits are possible, since there is a strong dependency of the eccentricity of the orbit on which SMC lies. Figure 7 confirms this dependency. In order to have two encounters between the Clouds as the recent star formation history suggests, the orbit of SMC around LMC needs to have an eccentricity between 0.6–0.7, otherwise it will decay too quickly in the LMC or it will be pushed away by its interaction with LMC halo.

As result of the selected orbit, figures 3 and 5 show the presence of an extending tail, a leading arm and a bridge of gas connected the two galaxies. The models also offer a good description of the Stream kinematic, showing a gradient of the line-of-sight velocity along the stream (Putman et al. 2003; Nidever et al. 2010).

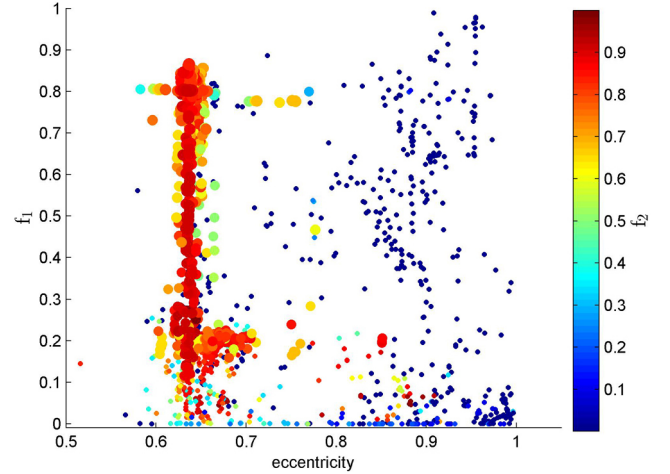
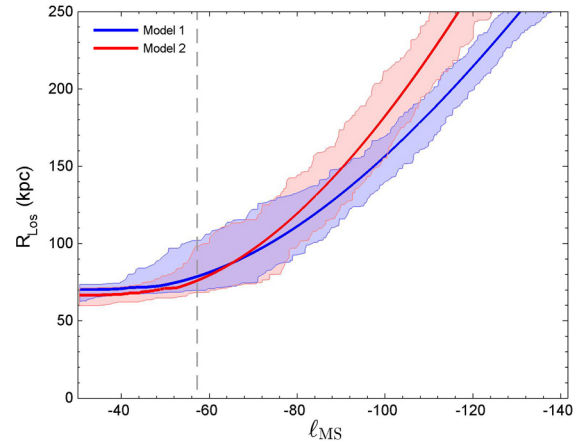
The formation mechanism of the stream is common in both models: the only interactions between the Clouds lead to the formation of the Magellanic System (Besla et al. 2010, 2012). The Clouds form a binary pair at least for the last 3 Gyr and the encounters between LMC and SMC are strong enough to strip material away from about 2 Gyr ago, mainly from the Small Cloud, in agreements with previous models (Connors et al. 2006; Diaz & Bekki 2012) and with the recent results from HST/COS and VLT/UVES (Fox et al. 2013).

ACKNOWLEDGEMENTS

Computational resources used in this work were provided by the University of Sydney High Performance Facilities.

REFERENCES

Battaglia G., Helmi A., Morrison H., Harding P., Olszewski E. W., Mateo M., Freeman K. C., Norris J., Shectman S. A., 2005, MNRAS, 364, 433

**Figure 7.** Dependence of the fitness function on the eccentricity. The results for the genetic algorithm show that f_1 term (today position and velocity of the Clouds) depends on the eccentricity of the SMC orbit around LMC. Each point on this plot shows how well a particular orbital solution is able to reproduce the present day position and velocity of the Clouds. The size of the points is scaled according to the values of the total fitness function, while the color of points indicates the value of the f_2 term (encounters between the Clouds at the time of the SFH).**Figure 9.** Fit of the distance along the Stream as function of ℓ_{MS} for Model 1 (blue) and Model 2 (red). The shared regions indicate the confidence interval, calculated from the bootstrap distribution in both models. The dashed line shows the direction of the SGP.

- Besla G., Kallivayalil N., Hernquist L., Robertson B., Cox T. J., van der Marel R. P., Alcock C., 2007, ApJ, 668, 949
 Besla G., Kallivayalil N., Hernquist L., van der Marel R. P., Cox T. J., Kereš D., 2010, ApJL, 721, L97
 Besla G., Kallivayalil N., Hernquist L., van der Marel R. P., Cox T. J., Kerevs D., 2012, MNRAS, 421, 2109
 Bland-Hawthorn J., Maloney P. R., Sutherland R. S., Madsen G. J., 2013, ApJ, 778, 58
 Bland-Hawthorn J., Sutherland R., Agertz O., Moore B., 2007, ApJL, 670, L109
 Boylan-Kolchin M., Bullock J. S., Sohn S. T., Besla G., van der Marel R. P., 2013, ApJ, 768, 140
 Brewer B. J., Lewis G. F., 2005, PASA, 22, 128
 Busha M. T., Wechsler R. H., Behroozi P. S., Gerke B. F., Klypin

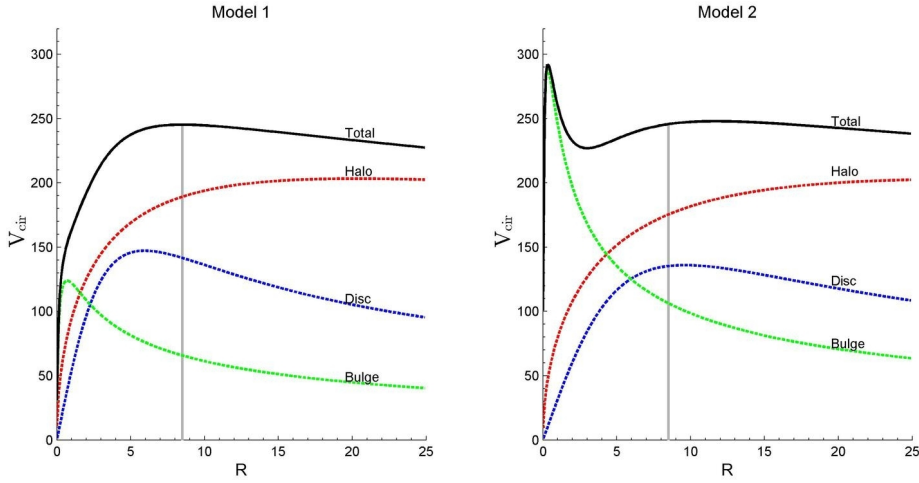


Figure 1. Rotation curve of the Milky Way for Model 1 (*left panel*) and Model 2 (*right panel*), shown for the contribution of each component (NFW halo, Miyamoto-Nagasai disc, spherical bulge) and the sum of them (total). For each model, the rotation curve due to the disc and bulge are fixed, while the halo contribution is chosen by the genetic algorithm. The adopted values for the virial mass of the halo are $0.99 \times 10^{12} M_{\odot}$ for Model 1 with concentration parameter of 27.3, and $1.27 \times 10^{12} M_{\odot}$ and concentration parameter equal to 20.5 for Model 2. In both panel, the solid grey line indicates the position of the Sun ($R_{\odot} = 8.5$ kpc) and its intersection with the total curve provides the circular velocity adopted for each model ($V_{\text{cir}} = 245.3 \text{ km s}^{-1}$ Model 1 , and $V_{\text{cir}} = 245.8 \text{ km s}^{-1}$ Model 2).

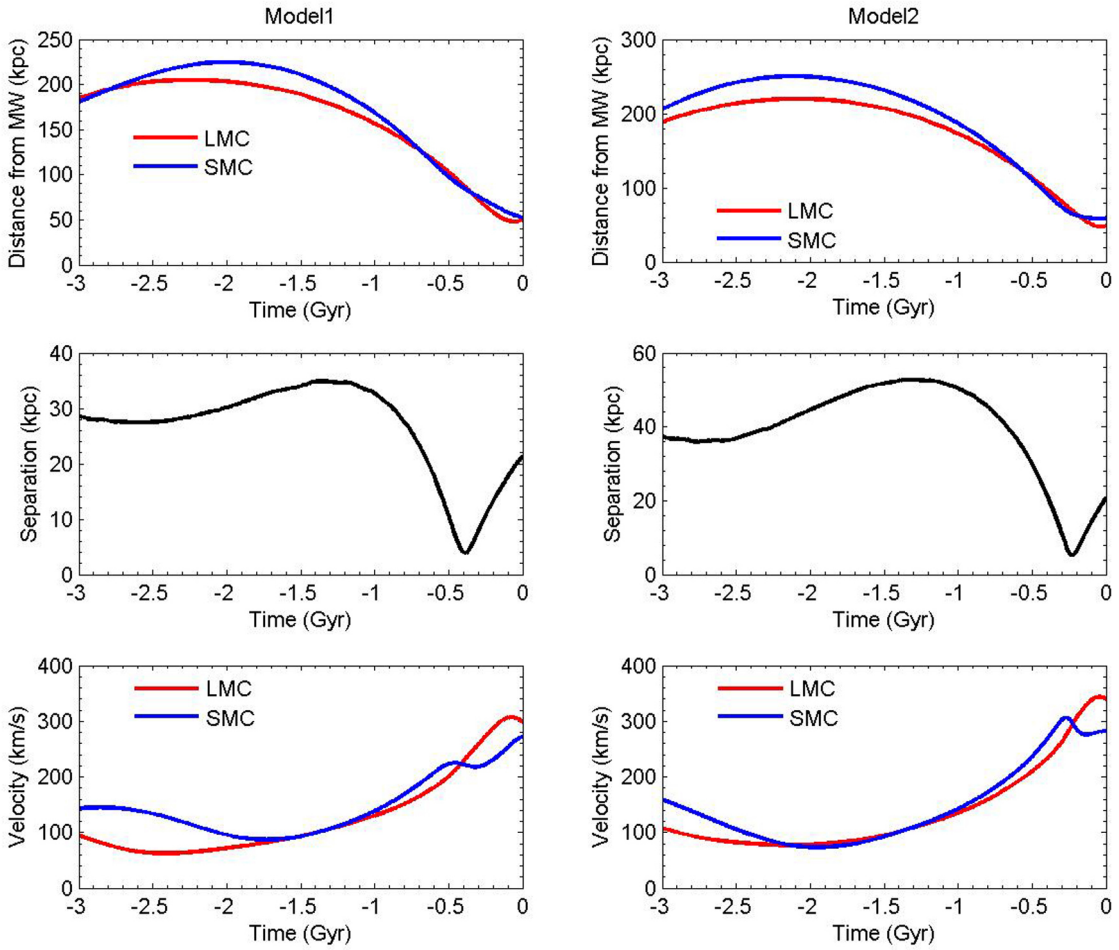


Figure 2. Orbit for the best individuals in Model 1 (*first column*) and Model 2 (*second column*). The first row of the figure shows the orbit of both Clouds around the Milky Way. In both cases, the Clouds are orbiting within the virial radius of the Milky Way for the last 3 Gyr. In the second row, the distance between LMC and SMC is plotted as function of time. The last row show the total velocity for both Clouds.

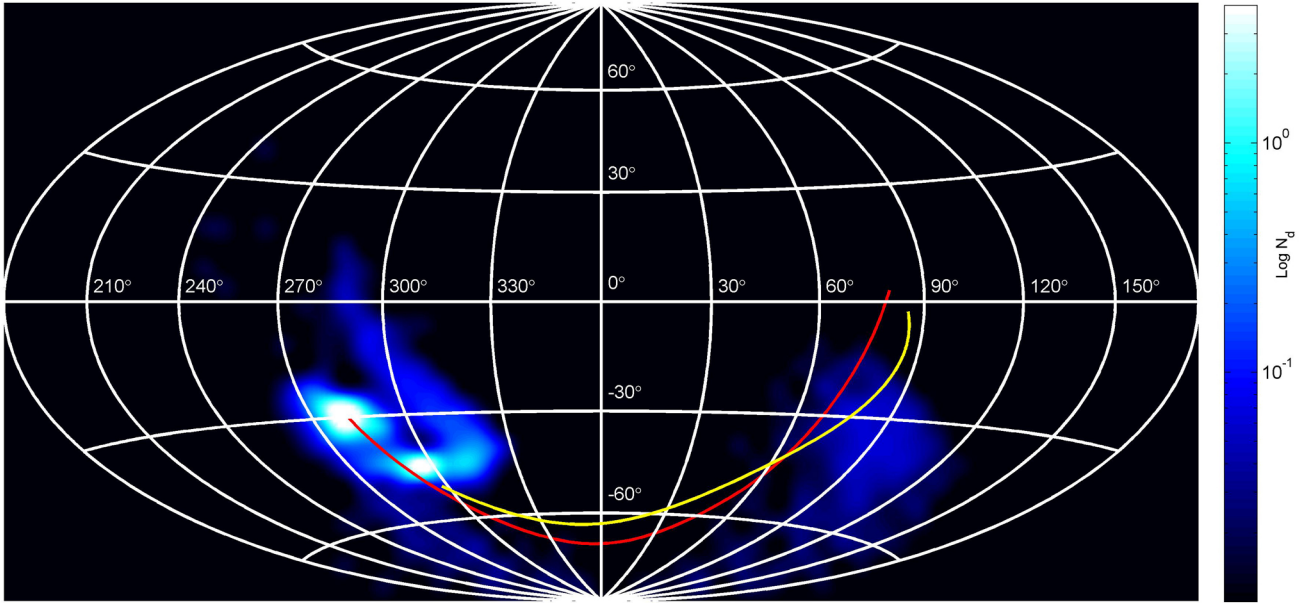


Figure 3. Aitoff-Hammer Projection of the only gas particles for Model 1, corresponding at $T = 0$. The solid red and yellow line are the projected orbit of LMC and SMC respectively in the last 1.5 Gyr, when the Stream starts to form.

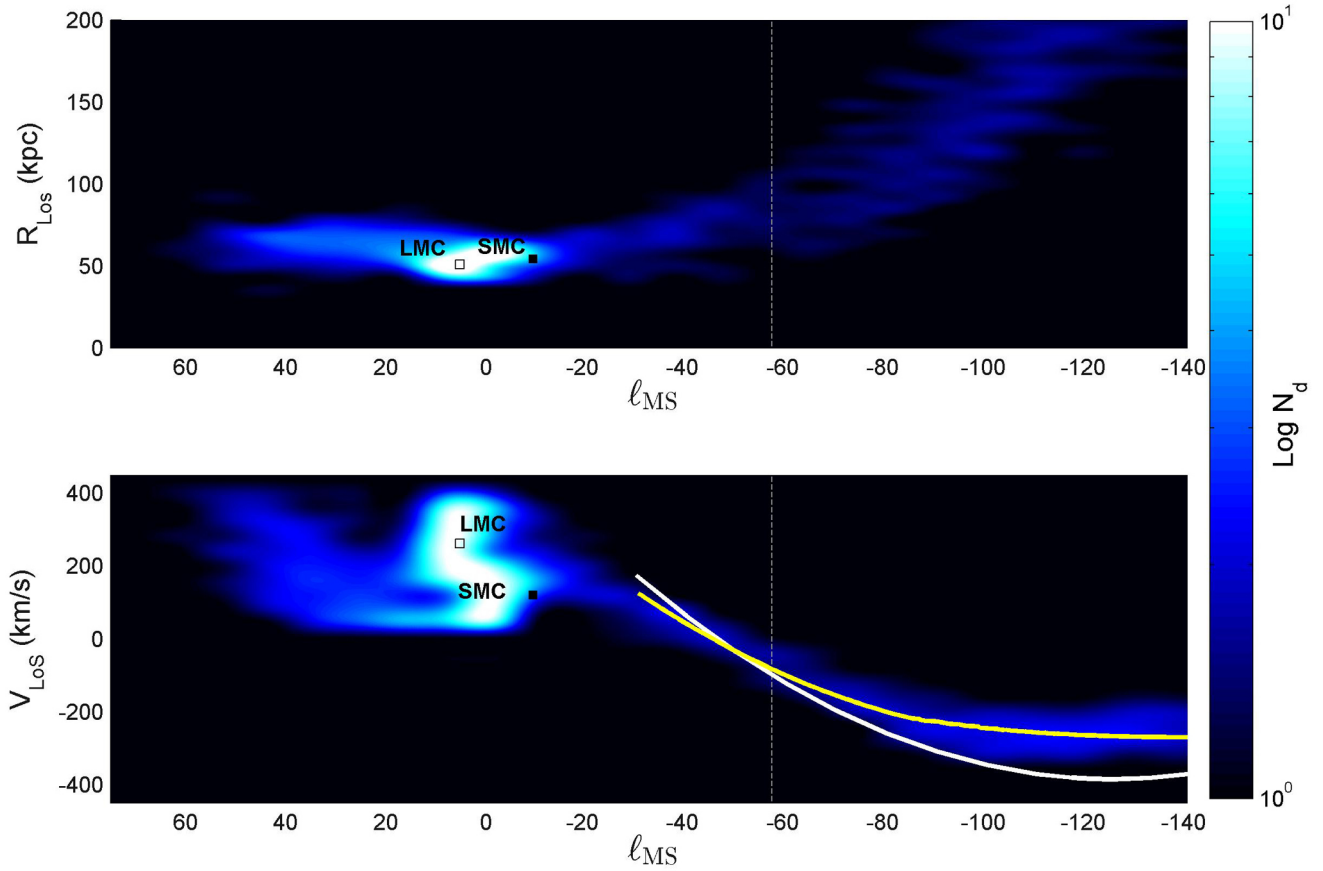


Figure 4. Model 1: line-of-sight distance (*Top Panel*) and line-of-sight velocity (*Bottom Panel*) for gas particles plotted as function of the Magellanic Longitude. The *white line* and *yellow line* show the result of a polynomial fit applied on the data from Nidever et al. (2010) *white line* and on the simulated data *yellow line*. In both panels, the *dashed line* indicates the direction of the South Galactic Pole.

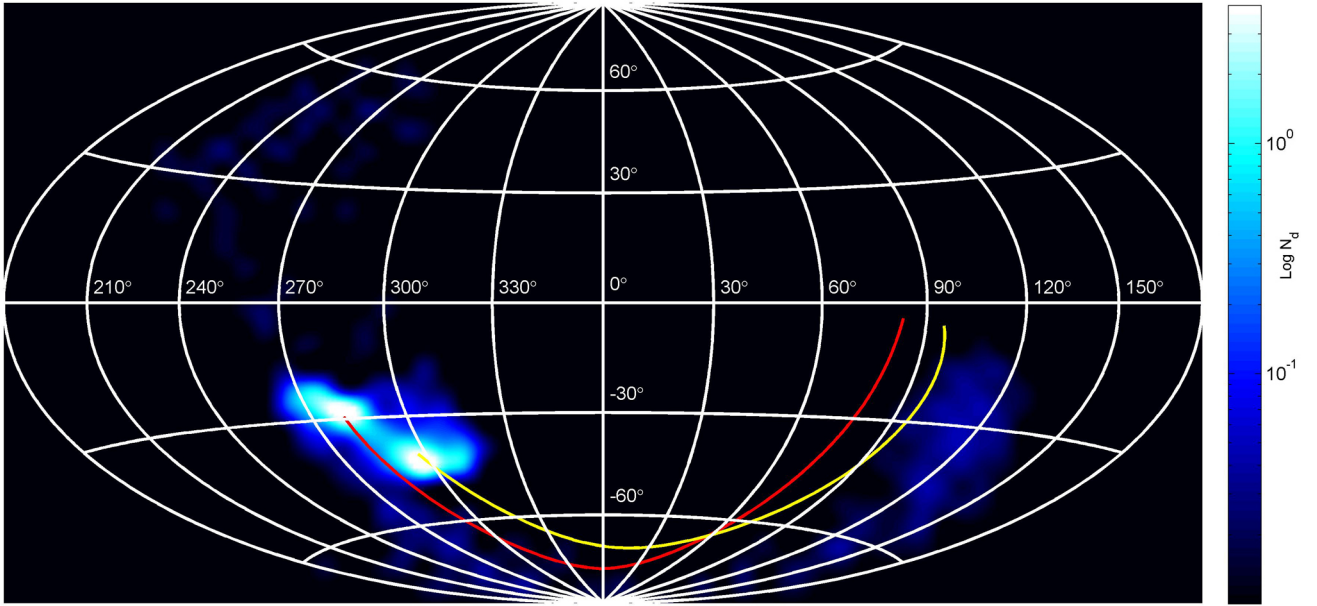


Figure 5. Aitoff-Hammer Projection of the only gas particles for Model 2, corresponding at $T = 0$. The solid red and yellow line are the projected orbit of LMC and SMC respectively in the last 1.5 Gyr, when the Stream starts to form.

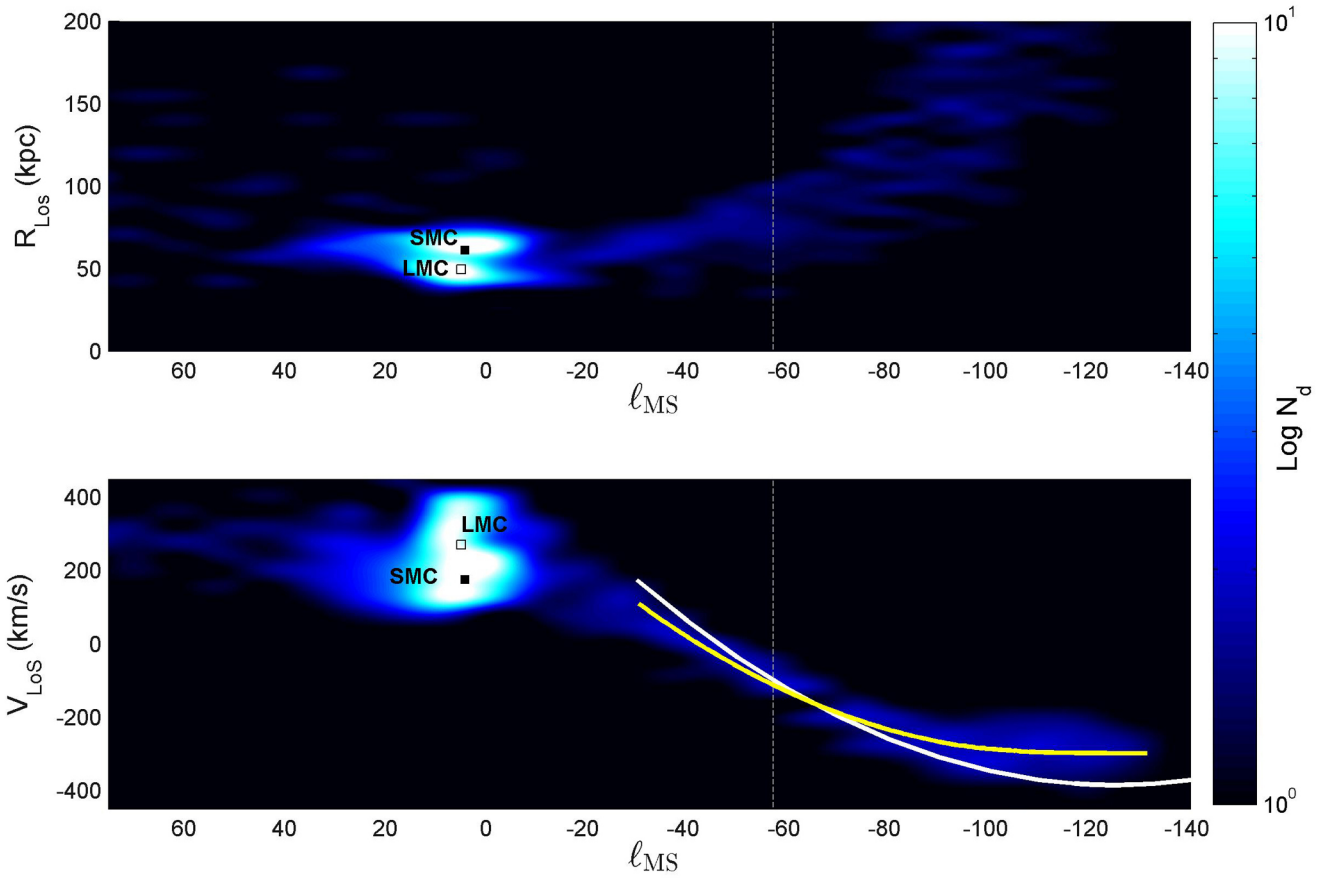


Figure 6. Model 2 results for the line-of-sight distance (*top panel*) and velocity (*bottom panel*) for gas particles plotted as function of the Magellanic Longitude. As in bottom panel in figure 4, in the *bottom panel*, the white line shows the fit on the data from Nidever et al. (2010), while the fit on the simulated data is plotted in yellow. The *dashed line* shows the direction of the South Galactic Pole.

	LMC	SMC	References
$m - M$	18.50 ± 0.1	18.95 ± 0.1	van der Marel et al. (2002), Cioni et al. (2000)
V_{sys} (km s^{-1})	262.2	146.0	van der Marel et al. (2002), Harris & Zaritsky (2006)
(α, δ) (deg)	(81.9, -69, 9)	(13.2, -72.5)	van der Marel et al. (2002), Smith et al (2007)
(l, b) (deg)	(280.253, -32.5)	(301.5, -44.7)	-

Table 2. Adopted value for the distance moduli, systemic velocity and Galactic Coordinates for both Clouds. These values are used for converting the velocity in the Galactic frame, in equation 9.

Parameters	Range	Model1	Model2	Referenced Value
M_{vir} ($10^{12} M_{\odot}$)	[0.90, 2]	1.00	1.27	Xue et al. (2008); Kafle et al. (2012)
c	[1, 30]	27.3	20.5	Battaglia et al. (2005); Deason et al. (2012) Rashkov et al. (2013), Kafle et al (2014)
$(\mu_{\text{W}}, \mu_{\text{N}})_{\text{LMC}}$ (mas/yr)	$(-1.89 \pm 0.27, 0.39 \pm 0.27)$	$(-1.87, 0.38)$	$(-2.03, 0.19)$	Vieira et al. (2010)
$(\mu_{\text{W}}, \mu_{\text{N}})_{\text{SMC}}$ (mas/yr)	$(-0.98 \pm 0.30, -1.10 \pm 0.29)$	$(-1.08, -1.04)$	$(-0.98, -1.20)$	Vieira et al. (2010)
Ω ($\text{km s}^{-1} \text{kpc}^{-1}$)	[28.0, 32.0]	30.3	30.3	McMillan & Binney (2010)
V_{cir} (km s^{-1})	-	245.3	245.8	McMillan (2011)

Table 3. Parameter range and genetic algorithm best values. The first and second columns describe the parameters used in the genetic algorithm with their range. Note that the circular velocity is not a free parameter, but it is calculated from the rotation curve, therefore it depends on the particular choice of the virial mass and concentration. The following columns describe the results for the two different models of the disc and bulge used in this work (see Tab. 4). The last column shows the referenced value for each parameter.

- A. A., Primack J. R., 2011, ApJ, 743, 117
Charbonneau P., 1995, ApJS, 101, 309
Cioni M.-R. L., van der Marel R. P., Loup C., Habing H. J., 2000, AAP, 359, 601
Connors T. W., Kawata D., Gibson B. K., 2006, MNRAS, 371, 108
Costa E., Méndez R. A., Pedreros M. H., Moyano M., Gallart C., Noël N., Baume G., Carraro G., 2009, AJ, 137, 4339
Deason A. J., Belokurov V., Evans N. W., An J., 2012, MNRAS, 424, L44
Diaz J. D., Bekki K., 2012, ApJ, 750, 36
Fox A. J., Richter P., Wakker B. P., Lehner N., Howk J. C., Ben Bekhti N., Bland-Hawthorn J., Lucas S., 2013, ApJ, 772, 110
Freeman K., Bland-Hawthorn J., 2002, ARA&A, 40, 487
Gardiner L. T., Sawa T., Fujimoto M., 1994, MNRAS, 266, 567
Gnedin O. Y., Kravtsov A. V., Klypin A. A., Nagai D., 2004, ApJ, 616, 16
Guo F., Mathews W. G., 2012, ApJ, 756, 181
Harris J., Zaritsky D., 2004, AJ, 127, 1531
Harris J., Zaritsky D., 2006, AJ, 131, 2514
Harris J., Zaritsky D., 2009, AJ, 138, 1243
Hernquist L., 1990, ApJ, 356, 359
James P. A., Ivory C. F., 2011, MNRAS, 411, 495
Jin S., Lynden-Bell D., 2008, MNRAS, 383, 1686
Kafle P., Sharma S., Lewis G. F., Bland-Hawthorn J., 2014, An observational constrained 3D model of the Milky Way Potential, submitted ApJ
Kafle P. R., Sharma S., Lewis G. F., Bland-Hawthorn J., 2012, ApJ, 761, 98
Kallivayalil N., van der Marel R. P., Alcock C., 2006, ApJ, 652, 1213
Kallivayalil N., van der Marel R. P., Alcock C., Axelrod T., Cook K. H., Drake A. J., Geha M., 2006, ApJ, 638, 772
Kallivayalil N., van der Marel R. P., Besla G., Anderson J., Alcock C., 2013, ApJ, 764, 161
Kuijken K., Dubinski J., 1995, MNRAS, 277, 1341
Lin D. N. C., Lynden-Bell D., 1977, MNRAS, 181, 59
Liu L., Gerke B. F., Wechsler R. H., Behroozi P. S., Busha M. T., 2011, ApJ, 733, 62
Macciò A. V., Dutton A. A., van den Bosch F. C., 2008, MNRAS, 391, 1940
Mastropietro C., Moore B., Mayer L., Wadsley J., Stadel J., 2005, MNRAS, 363, 509
McMillan P. J., 2011, MNRAS, 414, 2446
McMillan P. J., Binney J. J., 2010, MNRAS, 402, 934
Miyamoto M., Nagai R., 1975, PASJ, 27, 533
Mo H. J., Mao S., White S. D. M., 1998, MNRAS, 295, 319
Moore B., Davis M., 1994, MNRAS, 270, 209
Murai T., Fujimoto M., 1980, PASJ, 32, 581
Navarro J. F., Frenk C. S., White S. D. M., 1997, ApJ, 490, 493
Nichols M., Colless J., Colless M., Bland-Hawthorn J., 2011, ApJ, 742, 110
Nidever D. L., Majewski S. R., Burton W. B., 2008, ApJ, 679, 432
Nidever D. L., Majewski S. R., Butler Burton W., Nigra L., 2010, ApJ, 723, 1618
Offer A. R., Bland-Hawthorn J., 1998, MNRAS, 299, 176
Putman M. E., Staveley-Smith L., Freeman K. C., Gibson B. K., Barnes D. G., 2003, ApJ, 586, 170
Rashkov V., Pillepich A., Deason A. J., Madau P., Rockosi C. M., Guedes J., Mayer L., 2013, ApJL, 773, L32
Reid M. J., Menten K. M., Zheng X. W., Brunthaler A., Moscadelli L., Xu Y., Zhang B., Sato M., Honma M., Hirota T.,

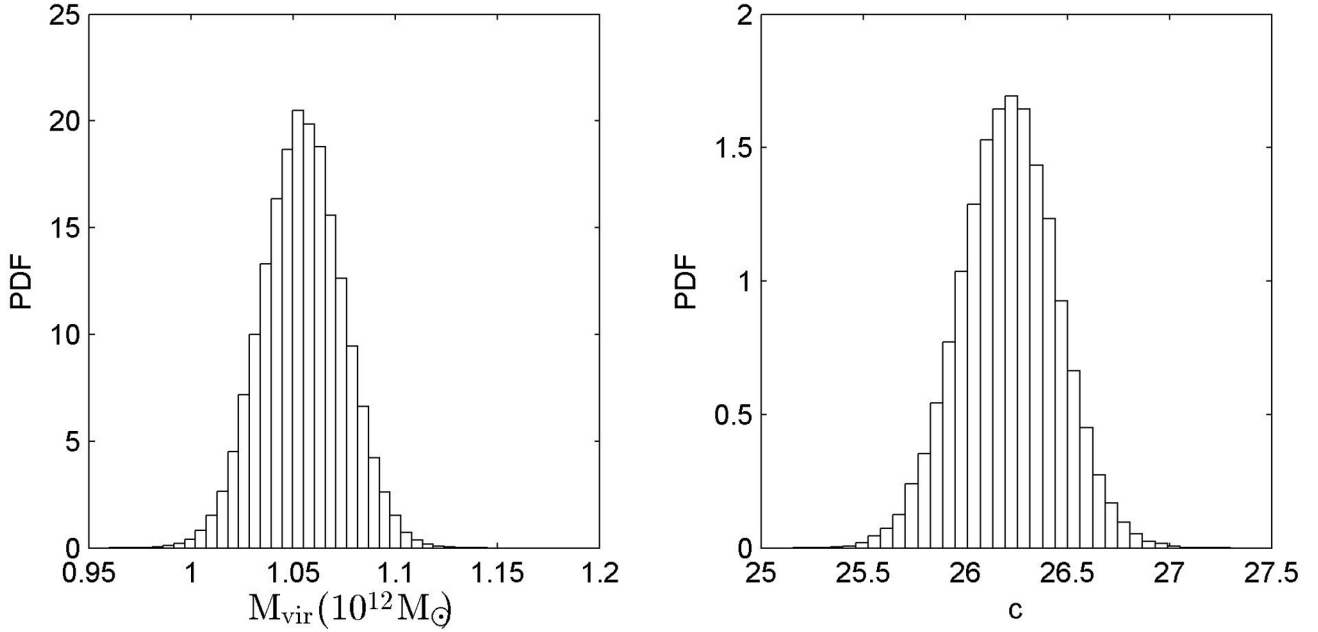


Figure 8. (From left to right) The marginalized distribution of the virial mass (M_{vir}) of the Milky Way and its variance ($\sigma_{M_{\text{vir}}}$) and the marginalized distribution for the concentration parameter, c .

- Hachisuka K., Choi Y. K., Moellenbrock G. A., Bartkiewicz A., 2009, *ApJ*, 700, 137
- Robotham A. S. G., Baldry I. K., Bland-Hawthorn J., Driver S. P., Loveday J., Norberg P., Bauer A. E., Bekki K., Brough S., Brown M., Graham A., Hopkins A. M., Phillipps S., Power C., Sansom A., Staveley-Smith L., 2012, *MNRAS*, 424, 1448
- Ruzicka A., Palous J., Theis C., 2007, *AAP*, 461, 155
- Ruzicka A., Theis C., Palous J., 2009, *ApJ*, 691, 1807
- Ruzicka A., Theis C., Palous J., 2010, *ApJ*, 725, 369
- Schönrich R., Binney J., Dehnen W., 2010, *MNRAS*, 403, 1829
- Shattow G., Loeb A., 2009, *MNRAS*, 392, L21
- Sohn S. T., Besla G., van der Marel R. P., Boylan-Kolchin M., Majewski S. R., Bullock J. S., 2013, *ApJ*, 768, 139
- Springel V., 2005, *MNRAS*, 364, 1105
- Theis C., 1999, in Schielicke R. E., ed., *Reviews in Modern Astronomy Vol. 12 of Reviews in Modern Astronomy, Modeling Encounters of Galaxies: The Case of NGC 4449*. p. 309
- Tollerud E. J., Boylan-Kolchin M., Barton E. J., Bullock J. S., Trinh C. Q., 2011, *ApJ*, 738, 102
- Toomre A., Toomre J., 1972, *ApJ*, 178, 623
- Tosi M., 2003, *Ap&SS*, 284, 651
- van der Marel R. P., Alves D. R., Hardy E., Suntzeff N. B., 2002, *AJ*, 124, 2639
- Vieira K., Girard T. M., van Altena W. F., Zacharias N., Casetti-Dinescu D. I., Korchagin V. I., Platais I., Monet D. G., López C. E., Herrera D., Castillo D. J., 2010, *AJ*, 140, 1934
- Wahde M., 1998, *AAPS*, 132, 417
- Widrow L. M., Dubinski J., 2005, *ApJ*, 631, 838
- Widrow L. M., Pym B., Dubinski J., 2008, *ApJ*, 679, 1239
- Xue X. X., Rix H. W., Zhao G., Re Fiorentin P., Naab T., Steinmetz M., van den Bosch F. C., Beers T. C., Lee Y. S., Bell E. F., Rockosi C., Yanny B., Newberg H., Wilhelm R., Kang X., Smith M. C., Schneider D. P., 2008, *ApJ*, 684, 1143
- Zhang X., Lin D. N. C., Burkert A., Oser L., 2012, *ApJ*, 759, 99